PRELIMINARY RESULTS OF SOUNDING CLOUDS AND THE UNDERLYING SURFACE OBTAINED WITH A SPACEBORNE LIDAR "BALKAN"

Yu.S. Balin, S.V. Samoilova, and A.I. Tikhomirov*

Institute of Atmospheric Optics and
**Design and Technology Institute "Optika"*
Siberian Branch of the Russian Academy of Sciences, Tomsk

In this paper we present preliminary results of measurements carried out in 1995-1996 with a Russian spaceborne lidar "Balkan" installed onboard the orbiting station "Mir", which is operated here since August 1995. This lidar is the first spaceborne lidar operated on a routine basis. We present here the basic specifications of the lidar and the orbiting station that may affect the lidar measurement results. We also consider some methodological aspects concerning the arrangement of the spaceborne experiments along with the analysis of some results on sounding the ocean surface, cloud fields, and the land obtained in different regions of the Earth under different conditions of solar illumination of its surface.

1. INTRODUCTION

Laser sounding of the Earth's surface and the atmosphere from space has been performed for the first time within the framework of American LITE[1] program in 1994. Experiments with the Russian spaceborne lidar "Balkan" have been conducted in August– September, 1995 and in February–April, 1996 from the orbiting station "Mir". In 1995 two station crews of the missions, EO-19 (N. Budarin and A. Solovjev) and EO-20 (Yu. Gidzenko and S. Avdeev), have serviced the lidar onboard the station. In 1996 the crew of EO-21 mission (Yu. Onufrienko and Yu. Usachyov) continued the spaceborne lidar experiment. The authors of this paper have contributed into the organization of the ground support of the missions at the Space Flight Center.

The primary goal of the spaceborne experiments conducted was mostly a technological test of the lidar operation ability, as well as the development of a technique for making the spaceborne and ground support measurements. These experiments were also aimed at achieving the task of verification and improvement of the ballistic techniques being used for orientation of the orbiting station. And finally we planned to acquire an array of lidar data on cloud formations and the underlying surface and to develop, using these data, a technique for their processing and interpretation.

2. MODES OF THE STATION "MIR" ORIENTATION ON THE ORBIT

In 1995 and 1996 the perigee of the "Mir" station orbit was 393 km and its apogee 413 km. The mean time of the station revolution around the Earth was 92.41 min at a 7.7 km/s mean speed of orbiting. The angle of the orbit plane inclination with respect to the equator plane was 51.74°.

As to the "Balkan" lidar specifications they have been described in detail in Refs. 3 and 4 therefore here we present only those which are needed for when planning experiments. Thus the period between successive laser shots was 5.53 s, the number of laser shots available in a single measurement cycle may be varied among 20, 60, or 80 per cycle. Each measurement cycle has to be followed by a 25-min interval for the laser head cooling. The sounding beam divergence was 0.15 mrad. As a result the distance between two spots on the Earth's surface was about 42.58 km and the maximum length of the band sounded was 3400 km. Lidar return signals were detected with a PMT operated in analog mode and then recorded with two devices operated in parallel.[3,4] The two recording devices make up two recording channels, i.e., the range finder channel and the lidar channel. In the former one the moments in time are recorded when the return signal intensity successively exceeds four threshold levels. The error of such range measurements is about 1.5 m. In the lidar channel we use a 6-bit ADC providing a 3-m spatial resolution of the lidar return recording. The operation of the lidar may be controlled either manually or in a semiautomatic mode (the lidar switching on is performed by a command from the onboard computer of the station and then an operator should provide a service for a 20-minute measurement cycle).

To provide a possibility of identifying the position of the station blocks as well as of the devices installed inside it and for orientation of the station itself two clockwise coordinate systems are used, one being related to the station and a basic one. The former has, by definition, its origin at the station center of mass with the axis $+O_bX_b$ coinciding with the symmetry axis of the main block of the station. This axis is directed backward of the flight direction at the stage of station approach the orbit after launching. The axis

0235-6880/97/03 209-12 $02.00

$+O_bX_b$ of this coordinate system is in the plane of the station cross section and it is directed toward one of the station fins. The axis $+O_bZ_b$ completes the system to make a clockwise one (see Fig. 1). Determination of the lidar optical axis position with respect to the station coordinate system is illustrated with Fig. 1 too. It is seen that the lidar optical axis is in the plane $+X_bO_bZ_b$ at an angle $\alpha = 1.5°$ clockwise from the axis $-O_bX_b$. Such a mismatch between the axes is due to the initial optical arrangement that presumably enables one to protect the lidar photodetector from the high power light flux reflected backward from the four surfaces of the optical window through which the sounding beam is directed out of the station. The optical axis of the window is collinear with the axis $+O_mY_m$ and $-O_bX_b$ axis of the station module.

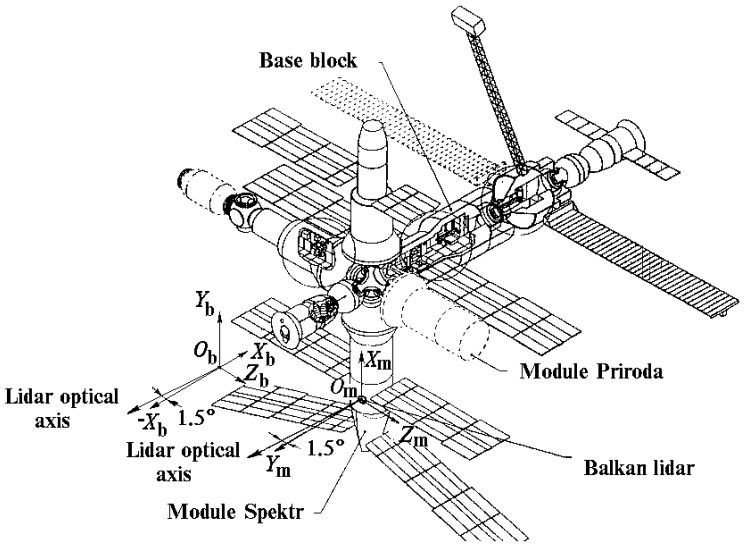

FIG. 1. The scheme of the lidar "Balkan" deployment in the "Spektr" module of the orbiting station "MIR" and position of the lidar optical axis in the coordinate systems coupled with the module and the main module of the station. The origin of the coordinate systems $O_bX_bY_bZ_b$ and $O_mX_mY_mZ_m$ are shifted off the corresponding centers of mass to better show the directions.

The basic coordinate system is used to set the station orientation in the inertial space. To describe the station motion two basic coordinate systems are used. Let us give their brief description omitting small details. First mention the inertial coordinate system (ICS) with the origin at the Earth's center. The axis $+O_iX_i$ is directed towards the equinoctial point position on January 1, 1985 at 3 am, decree Moscow time. The axis $+O_iZ_i$ is perpendicular to the plane of the mean equator and looks at the northern pole of the Earth. The axis $+O_iY_i$ completes this coordinate system make it clockwise. The second basic system is the orbital coordinate system (OCS) with the origin at the station center of mass, with its axis $+O_oX_o$ directed along the velocity vector projection onto the plane of local horizon, and the axis $+O_oY_o$ directed along the radius-vector of the station (radius vector of the Earth) and the axis $+O_oZ_o$ completes the clockwise coordinate system.

Orientation of the orbiting station may be performed following different modes used to orient the station in the ICS and OCS depending on the angle between the station and a basic coordinate systems.[5] In the measurement cycles with the lidar two modes of orientation were employed designated as ICS2 and OCSc. The orientation mode ICS2 is the basic for use during the station flight, because it provides better power supply for the station from its solar batteries. In this mode the axis $+O_bX_b$ is aligned along the projection of the direction towards the Sun onto the orbit plane while the $+O_bY_b$ axis is directed so that it is normal to the orbit plane and makes a minimal angle with the direction toward the Sun.

The scheme presented in Fig. 2*a* illustrates the station flight in ICS2. Since in this orientation mode the $+O_bX_b$ axis is permanently looking at the Sun, the angle between the lidar optical axis and nadir direction also changes. This results in a continuous scanning with the laser beam in the orbit plane. As a consequence the lidar optical axis approaches nadir only for a short time in the middle of the illuminated portion of the orbit when the $+O_bX_b$ axis approaches the direction toward the Earth's radius vector (with the account for the instrumental mismatch of 1.5°). It is obvious that in this case (the side illuminated by the Sun) the background noise conditions are most unfavorable for lidar operation. At the same time it is impossible, under this orientation mode, to perform sounding of the atmosphere at the dark side because here the lidar looks at the outer space.

In the orientation mode OCSc the station, together with the lidar, is oriented, at some moment in time, along a desired direction and this orientation is then stabilized during the entire cycle of the lidar experiment. After the experiment the station is oriented back to the initial orientation according to the ICS2 orientation mode. The OCSc mode of the station orientation enables a desired orientation to be set at any time and any portion of a revolution (see Fig. 2*b*), because the lidar optical axis is directed along the

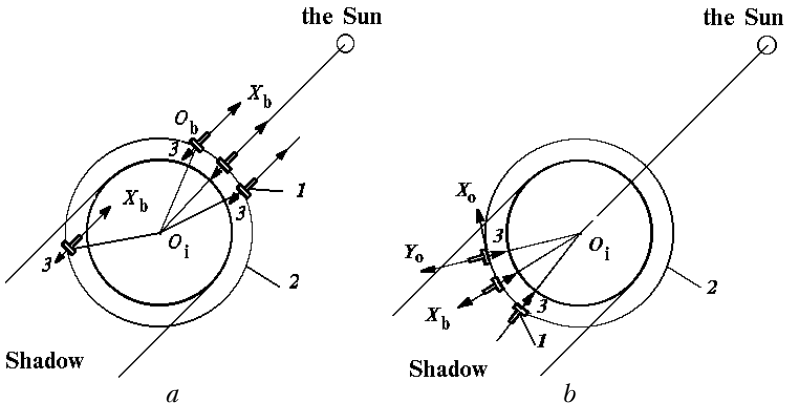

FIG. 2. The modes of the station orientation on its orbit: 1 is the station; 2 is the orbit; 3 is the lidar optical axis; O_i is the center of the inertial coordinate system (the Earth's center); $O_oX_oY_oZ_o$ is the orbital coordinate system. a) is the ICS2 orientation mode; b) is the OCSc orientation mode.

$-O_oY_o$ axis of the OCS and the $+O_bX_b$ axis makes only 1.5° angle with the axis $+O_oY_o$. However this mode needs for an amount of fuel to provide reorientation and maintenance of its stability.

3. ORGANIZATION OF THE LIDAR EXPERIMENTS

3.1. Planning of the spaceborne experiment. The ground support of lidar experiments involves: 1) long- and short-term planning at the space flight center (SFC); 2) organization of accompanying ground support measurements; 3) arrangement of accompanying photometric measurements or photographing.

Given that the station flight is well determined the planning assumes a choice of geographical regions for future survey and making preliminary ballistic calculations at the SFC for predicting the time when the station is over the region desired including calculation of the deviations in the geographical coordinates of such regions. The illumination conditions at the moments in time when lidar experiments are planned are also precalculated (elevation angle of the Sun and the Moon phases). In so doing the calculations are made with the account for timetable of the astronauts work (time for sleeping, meals, time to have a rest).

The long-term planning (5 days beforehand) takes into account the timetable of the crew, including their engagement in regular servicing, and the time of the station being over the desired regions is refined (especially if the orbit corrections are to be done) and the moments for the station reorientation according to the OCSc mode are calculated. It also involves the meteorological forecast to predict the presence of clouds.

The short-term planning (2 days beforehand) includes preparing and transfer of input data for the onboard computer to be able to send proper commands to switch on the lidar and corresponding systems of the station necessary for the lidar experiment at a proper time. Finally a message is composed for the crew which involves information on time to switch on the laser, the number of shots per measurement cycle, instruction about the instrumentation failures, and so on.

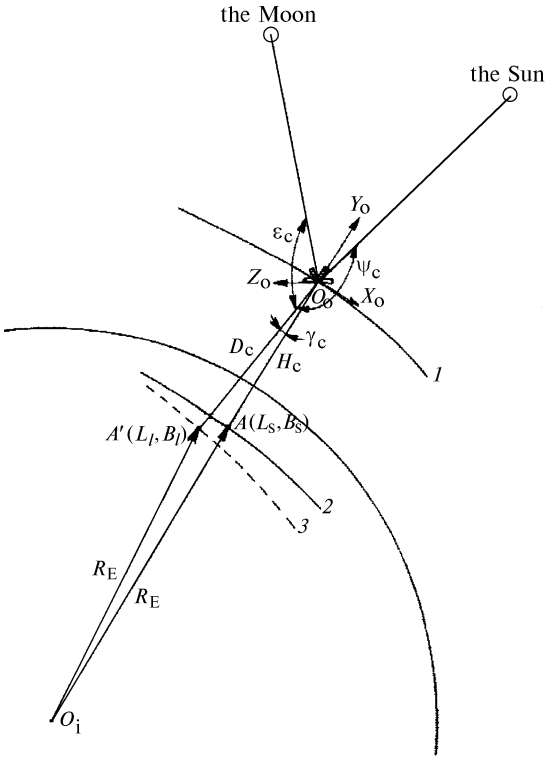

FIG. 3. Parameters of the station orbit and of the lidar orientation: 1 is the orbit portion; 2 is the calculated orbit track on the Earth's surface; $O_oX_oY_oZ_o$ is the orbital coordinate system; O_i is the center of the inertial coordinate system; R_E is the Earth's radius-vector.

3.2. Ballistic calculations in support of the lidar experiments. Figure 3 explains the parameters of the flight trajectory calculated, as well as of the lidar orientation and of the regions on the Earth's surface sounded. The origin of the inertial coordinate system,

O_i, is at the Earth's center, while that of the orbital coordinate system $O_oX_oY_oZ_o$, is at the station center of mass. In the general case the trajectory of the laser spots on the Earth's surface doesn't coincide with the projection of the flight trajectory even in the OCSc orientation mode because of the uncertainties in the calculated direction of the lidar optical axis, certain errors and fluctuations of the station orientation. In the SFC there are computer programs that allow one to calculate current values of the orbit height above the ocean surface, $H_c(t)$ (segment O_oA'), with the account for the geoid shape. There are also programs for computing geographical coordinates, the longitude $L_s(t)$ and the latitude $B_s(t)$ of the point A (just below the satellite), the predicted distance along a slant path $D_c(t)$ (segment O_oA') at a preset angle γ_c between the lidar optical axis and nadir, geographical coordinates of the point A′ where the lidar optical axis intersects the Earth's surface $L_1(t)$ and $B_1(t)$, the angles between the lidar optical axis and the direction towards the Sun $\psi_c(t)$ and the Moon $\varepsilon_c(t)$. All these calculations use the data of the radar monitoring of the station orbit, which is being done every day. These data are then used when interpreting lidar data.

3.3. Ground support measurements. In order to improve the reliability of the lidar returns interpretation it is desirable to have data of accompanying ground support measurements of the atmospheric parameters, parameters of clouds and the underlying surface. In the first version of the lidar in space program it was planned to arrange synchronous ground support measurements from an aircraft and ships in the region surveyed from space. To meet this requirement we have specially designed an airborne lidar.[6] However, we have managed to conduct correlative measurements of the cloud fields only in September 1995 over one region in the northern Atlantic with this special lidar installed onboard the research vessel "Akademik Mstislav Keldysh." It should be noted that at the present state of this research the value of such correlative experiments is too problematic because the measurement sites are wide apart while the spatial gradients of the optical properties of the atmosphere are high enough.

In addition to the ground support measurements meteorological situation (presence of clouds and their amount) on the territories under the orbiting station may be observed and assessed visually by any other astronaut and/or using an automated videocamera. However, such observations can be performed only on the illuminated side of the Earth, i.e., under conditions most unfavorable for lidar sensing.

The low inclination of the station orbit, 52°, doesn't enable simultaneous ground-based sensing to be done using lidar stations in Tomsk and Minsk which are 600 and 200 km to the North from the extreme northern point of the station trajectory. Moreover, the territories near these points were far out of the areas observed from the station during the periods planned at the SFC for lidar experiments.

The state hydrometeorological center supplies the SFC with the short-term weather forecasts before a spaceborne lidar experiment and with the data of standard meteorological observations in the regions surveyed after it. In the latter bulk of meteorological information there are data on the cloud types, their amount, low boundary of the cloudiness, and on the wind velocity over the regions under the flight trajectory. However, the information on cloud fields is not so valuable as regards widely spaced sounding paths of the spaceborne lidar.

3.4. Arrangement of the lidar measurement sessions. At present all crews of the manned orbiting station (starting with the EO-19 mission) are trained to work with the lidar "Balkan" at the SFC training center. In addition, there is a detailed instruction manual for operators onboard the station. And finally the operator receives concrete instructions concerning a particular lidar experiment from the radio message just before its beginning.

In a semiautomatic mode of operation an operator takes control over the lidar facility 10 minutes before the experiment by checking from the lidar control board its functional ability. Then he or she switches on the lidar at a prescribed time to emit sounding pulses in a series or single-pulse mode. After that the operator switches off the lidar and enters the lidar data acquired to the onboard tape recorder of the telemetric system of the station.

3.5. Telemetric messages. The telemetric message with the information acquired with the lidar "Balkan" consists of two parts. The first one is the array of digital data on the lidar returns recorded and the measurement certificate while the second portion of this telemetric message contains analog signals from the telemetric control system on the functioning of different blocks of the lidar. The latter portion of the message also contains information on the range D_m measured with the range finder channel at the first amplitude threshold.[3,4]

During each session digital arrays of telemetric information are compiled in the buffer storage device of the lidar channel. The response signals of the telemetric control are recorded on the onboard tape recorders of the station that allows one to make objective analysis of the operator actions during the measurement session.

All the telemetric information acquired during a lidar measurement session is then transmitted to one of the ground station that receives it when the station flies over it. Thus collected data are then transferred to the SFC. Preliminary decoded telemetric information is presented to the experimenter at the SFC in 1 or 1.5 hours after the measurement session.

3.6. Data acquisition and processing. While making an operative processing of the telemetric messages from the orbiting station at SFC first the information related to lidar experiments is extracted. The signals from the telemetric control system that are given to the experimenter in printed form enable analysis of all successive operations done with the lidar in the experiment conducted. The arrays of digital data on lidar returns are then restructured to take a file form, accessible for further processing on a computer in order to extract information on the shape of lidar returns

and its certificate data in each measurement session.

Preliminary processing of the data from the range finder channel involves a comparison between the data obtained with the lidar, D_m, and calculated values of the slant range $D_c(t)$ and elimination of false records due to the background noise from the data array. The false records occur when the noise amplitude exceeds the first threshold level and thus enters the time gate of the time-to-code converter. There are two criteria used to identify the false records. According to one the data are rejected if D_m exceeds the value D_c by the amount exceeding the measurement error or, according to the second one, if D_m is smaller than the value (D_c– 12 km) what corresponds to return signals from false objects at heights above 12 km. As the results of the experiments conducted have shown there are about 50% false records due to the noise when working on the illuminated side of the Earth. Similar false records took place when working on the dark side of the Earth also, but they comprised only 3% of the total number of records and only when the Moon phase exceeded 0.9. No return signals were recorded from thin cloudiness since in this case the amplitude of lidar returns didn't exceed the threshold. In addition the information is taken into account from meteorological bulletins on the presence of clouds over the regions surveyed as well as exact geographical coordinates of the laser spots on the Earth's surface along the projection of the flight trajectory in order to properly allow for the relief, when sounding the land.

When making preliminary data processing we first isolate, from the array of digital data, the lidar returns in the succession between two calibration signals recorded before and after the lidar measurement session. Then we isolate, from this portion of the file, the return signals that exhibit the range to the objects detected and have the certificate parameters close to that in the range finder channel. Thus digitized lidar returns are then used to determine the parameters of the scattering objects by employing certain algorithms.[4]

3.7. Spatiotemporal positioning of measurements. As the comparison made between the slant ranges to the ocean surface, D_m, obtained from the lidar data and those calculated from ballistics ($D_c(t)$) has shown there is a systematic error in the determination of the angle α ($\Delta\alpha \approx 0.3°$). Figure 4 presents the calculated dependence of the excess in the range measured with the lidar, $\Delta D = D_c - H_c$, on the angle between the lidar optical axis and nadir γ at a realistic height of flight of 400 km. It should be mentioned that the value D_c includes, in addition to the quantity $H_c/(1/\cos\gamma - 1)$, the excess in the slant range due to spherical shape of the Earth, which reaches significant values at $\gamma > 3°$.

As preliminary analysis of the data on stability of the station orientation has shown there occur oscillations of the station orientation relative to the basic coordinate system. In the ICS and OCSc orientation mode such oscillations can reach $\pm 0.1°$ during 10 minutes, that, in fact, introduces no essential errors into the height determination (about $\pm$ 0.5m) while significantly shifting the laser spot compared to its position (by more than 600 m) at nadir orientation of the lidar optical axis. As is seen from Fig. 4 the value ΔD essentially increases with increasing angle γ, the systematic error $\Delta\alpha$ being constant. Because of the uncertainty in $\Delta\alpha$ value ($\Delta\alpha \approx 0.3°$) actual coordinates of the laser spot on the Earth's surface are shifted relative to their calculated values $L_1(t)$ and $B_1(t)$ (see Fig. 3).

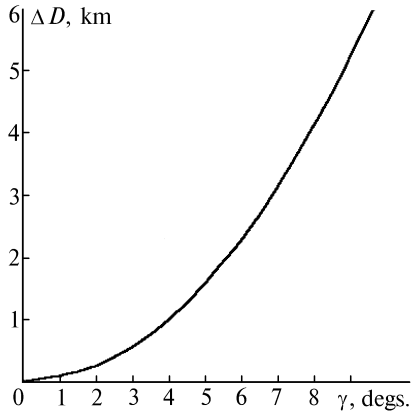

FIG. 4. The excess in the slant range as a function of the lidar axis deviation angle from nadir direction.

The uncertainty in determining the coordinates of the lidar sounding paths can also occur due to uncertainties in the onboard timing of measurements which is then reduced to the universal scale of Moscow time. Besides, when telemetric information is recorded on the onboard tape recorders a one second uncertainty appears since this process uses a one-second time scale. That immediately results in a $\pm$ 3.9-km uncertainty in the coordinates of the laser spot on the Earth's surface. The error in recording the time of a single measurement in the telemetric system is 0.5 s. Additional discrepancy between the values D_c and D_m occurs due to the errors in radar measurements of the station orbit from the Earth. Thus in the northern hemisphere the uncertainty in H_c value can reach 150 m while in the southern hemisphere it can be larger since no points of the radar control of the orbit is available there. The matter is that all ballistic calculations of the trajectory are referred to the time moment T_c and the longitude L_c when the projection of the orbit trajectory crosses the Earth's equator and therefore the one-second error in timing makes a 20 to 30 m error in the orbit height and that leads to a shift in the coordinates of the station projection point up to 8 km.

In fact a detailed analysis of the uncertainties in determination of time and coordinates of a particular spaceborne lidar experiment could be a subject for a separate publication, therefore we do not present it in this paper. Moreover, some estimates of such measurement errors caused by slopes of the reflecting surfaces and deviations of the lidar line of sight from nadir can be found in Ref. 8.

4. ALGORITHM OF THE LIDAR DATA INTERPRETATION

The general scheme of the lidar data processing involves the completion of the following tasks. First filtration of return signals against noise, then classification of the scattering objects has to be done, and finally the parameters of the objects detected should be reconstructed from these signals.

As the criteria for making classification we have chosen some significant and independent characteristics of lidar returns that can provide reliable identification of the scattering objects sounded. These characteristics are the length of the leading edge of the lidar return, the range to the object, and the S-function of the lidar return.

These characteristics bear information on the physical state of the object under study, since their values could be of a special interest in meteorology, climatology as well as for further development of the techniques to calculate the orbit parameters. Among such characteristics there are the height of the upper cloud boundary or the level of the underlying surface, optical parameters of clouds and the underlying surface. For instance, the integral S-function is directly related to the reflection properties of clouds and the underlying surface.

Assuming linear increase of the scattering coefficient $\sigma(z)$ we have

$$\frac{ds}{dz} = \frac{1}{2(z_m - z_0)^2} = \ln \frac{(z_2 - z_0)}{(z_1 - z_0)} [(z_2 - z_0)^2 - (z_1 - z_0)^2]^{-1},$$

that means that the function $\sigma(z)$ is related to the gradient $d\sigma/dz$. A stable estimate of the latter may be obtained by the least squares method, i.e.,

$$\frac{\hat{d}\, s}{dz} = \int_{z_1}^{z_2} \ln \frac{(z - z_0)\, S(z_m)}{(z_m - z_0)\, S(z)} [(z - z_0)^2 - (z_m - z_0)^2)]\, dz \times$$

$$\times \left\{ \int_{z_1}^{z_2} [(z - z_0)^2 - (z_m - z_0)^2]^2\, dz \right\}^{-1}.$$

Here z_0 and z_m are the ranges corresponding to the beginning and the maximum of a return signal; z_1 and z_2 are the ranges where to the points in the leading and the trailing edges of the return signal where it has the same value ($z_1 < z_2$).

As was shown in model calculations and then confirmed by the experimental data obtained the solution stability is poorer if we use, when processing, trailing edge of the return signals. If, in addition, we take into account the fact that this portion of return signals contains the noise due to multiple scattering we may recommend that only the leading edge of a signal should be used for estimating the mean value of the scattering coefficient of a cloud.

As noted above the recording system of the lidar "Balkan" is equipped with a range finder channel which is operated in parallel with the lidar channel. Its operation is based on a multithreshold principle that enables, using an approximation, to reconstruct the lidar return shape and then use it in data processing. It should be noted here that the return signals from clouds and water surfaces have a particular asymmetric shape, while those from hard surfaces are usually symmetric. However, if the sounding path direction deviates from nadir or the beam impinges a slant surface the shape of return signal is slightly asymmetric. As was shown in the overview[8] the signal broadening bears information on the surface inclination while the return maximum on the reflection coefficient.

5. GENERAL DESCRIPTION OF THE SPACEBORNE EXPERIMENTS CONDUCTED

The freedom in choosing the regions for lidar studies have been too limited in these experiments by the necessity of taking into account the orientation modes available during the "Mir" station flight and the timetable of the station crew work. Figure 5 shows the geographical regions over which we have managed to carry out the experiments. For example, in this figure is set out a projection of the station orbit onto the Earth's surface (for one revolution) starting from the longitude $L = 103°$. The dashed line in this figure depicts a portion of such a projection for the next revolution. Solid lines show the segments of the orbit projections denoting the regions over which the lidar experiments were conducted in 1995 (omitting necessary test sessions we have carried out 16 measurement sessions, three of which have been conducted in the OCSc orientation mode over the night side of the Earth). The dot-dash lines in the figure show the regions over which the lidar experiments have been carried out in 1996. The majority of lidar sensing sessions were over the region south-east of Labrador, where the ground support measurements from ship have also been carried out. In the latter series of lidar experiments we have managed to perform 17 measurement sessions of which 8 sessions have been carried out in the OCSc orientation mode, when we sounded the ocean surface and the underlying surface of the Australian desert.

In Table I one can find a brief description of the spaceborne experiments carried out in 1995. The table also gives information on the date and time (hour:min:sec, decree Moscow time) of the experiments and on the number of measurements in a session, as well as on the number of reliable range finder measurements rationed by the number of false responses due to the background noise (rel.meas./ false resp.). Figures in brackets, in this same column, show the number of returns recorded from clouds in the measurement session. Note that the sum of figures in the nominator and the denominator is less than the total number of measurements in the majority of cases. This is explained by the fact that

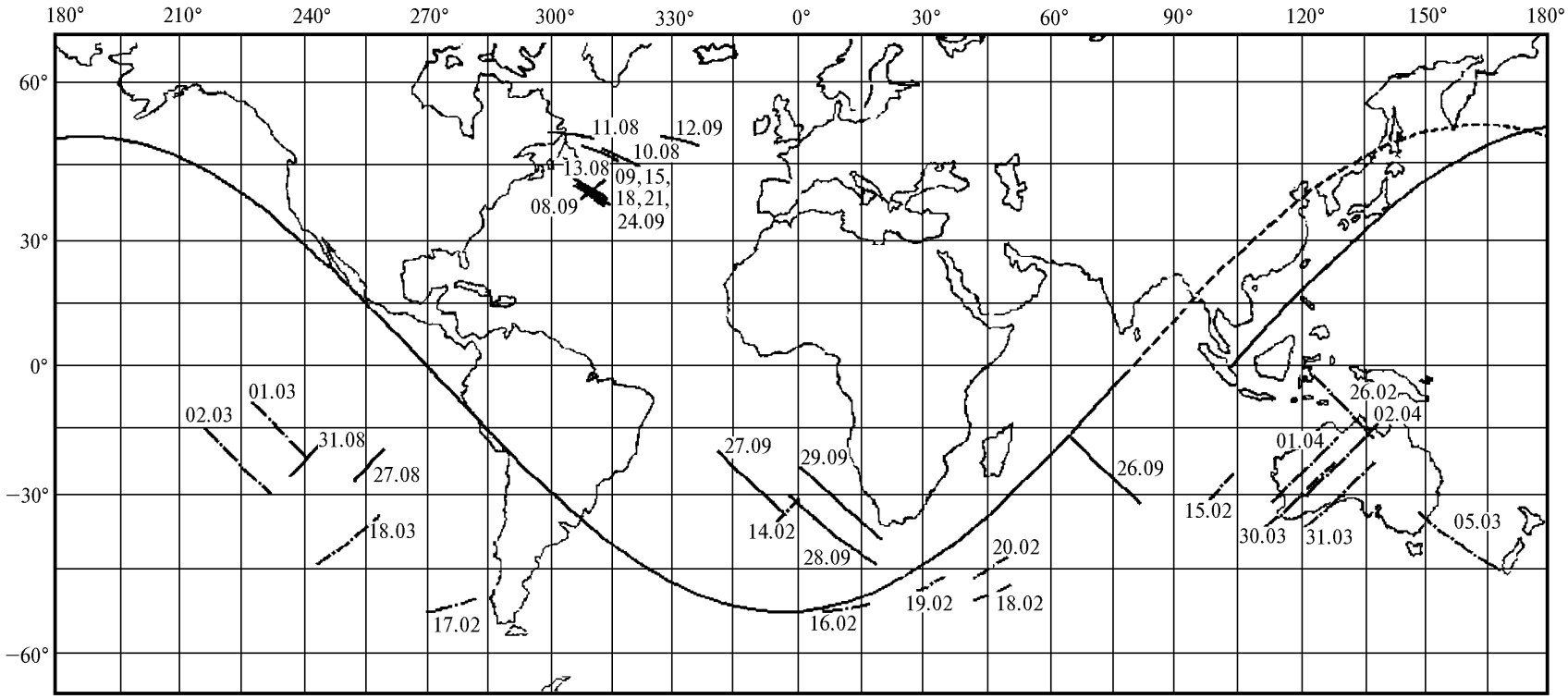

FIG. 5. Geographical regions surveyed with the "Balkan" lidar. The segmented lines show the flight track on the Earth's surface.

in some measurement cycles the amplitude of the return signals didn't reach even the first amplitude threshold of the range finder recording channel, because of weakly scattering clouds.

TABLE I. Information on the experiments (1995).

No.	Date	Time (DMT) start / end	Number of cycles	Rel. meas. / false resp. (returns from clouds)	Orientation mode	Coordinates B_s, degs.	Coordinates L_s, degs.	Cloudiness	The Sun elevation angle*	Remarks
1	10.08.95	09:11:29 / 09:13:14	20	19/0 (0)	OCSc	48.67 / 45.91	312.37 / 321.10	moderate	< −15.0	Enhanced voltage at PMT
2	11.08.95	08:13:55 / 08:15:40	20	20/0 (11)	»	51.72 / 50.82	298.80 / 309.13	»	< −15.0	»
3	13.08.95	08:01:30 / 08:03:15	20	20/0 (4)	»	49.74 / 47.36	307.34 / 316.53	dense	< −15.0	»
4	27.08.95	21:04:00 / 21:05:45	20	??	ICS2a	−27.73 / −19.65	251.64 / 256.13	–	–	No telemetric information
5	31.08.95	20:33:55 / 20:35:40	20	9/2 (2)	»	−22.04 / −16.88	237.98 / 242.29	moderate	41÷48	–
6	08.09.95	16:48:22 / 16:50:07	20	16/0 (2)	ISC	39.50 / 43.35	306.37 / 313.45	dense	48÷49	–
7	09.09.95	22:20:19 / 22:22:04	20	11/2 (0)	»	44.16 / 40.43	305.73 / 313.01	»	28÷23	–
8	12.09.95	18:01:09 / 18:02:54	20	4/8 (1)	»	50.93 / 49.15	327.67 / 337.47	thin	42÷20	–
9	15.09.95	20:01:46 / 20:03:31	20	18/0 (0)	»	42.90 / 39.00	307.81 / 314.78	dense	45÷44	–
10	18.09.95	18:51:31 / 18:53:16	20	9/0 (0)	»	43.84 / 40.07	305.58 / 312.79	»	48÷50	–
11	21.09.95	17:41:42 / 17:43:27	20	7/3 (1)	»	43.75 / 39.97	305.55 / 312.73	moderate	45÷50	–
12	24.09.95	16:32:26 / 16:34:10	60	16/1 (0)	»	43.05 / 39.21	306.74 / 313.68	»	39÷46	–
13	26.09.95	11:59:59 / 12:05:25	60	5/8 (2)	»	−15.47 / −31.11	63.90 / 78.29	»	65÷43	–
14	27.09.95	17:16:00 / 17:21:26	60	4/19 (3)	»	−17.18 / 32.59	339.08 / 353.82	»	69÷47	–
15	28.09.95	16:25:56 / 16:31:20	60	1/16 (1)	»	−28.86 / −42.29	357.41 / 16.05	»	57÷34	–
16	29.09.95	15:29:57 / 15:35:22	60	0/14	»	−23.40 / 37.91	359.80 / 16.42	»	68÷46	Laser warm up failure

* No data are available on the Moon in first experiments.

One can also find in this table information on the orientation modes of the station in the experiments and on the coordinates (longitude and latitude) of the starting and final point of the ground support measurements carried out simultaneously with the spaceborne lidar experiment (see Fig. 3). The table also gives information, though in a generalized form, on the cloudiness occurred, data on cloud amount and on the heights of the low and upper boundary of clouds were taken from bulletins of the State Hydrometeorological Center. To provide information about the illumination background conditions there are given in the table the elevation angles of the Sun and the Moon (for measurements on the dark side) at the beginning of measurements and at their end. The elevation angles refer to the local horizon in the localities over which the station flew during the measurements.

The measurement session of a series of 20 sounding pulses takes 105 seconds and that of 60 pulses takes 326 seconds. When making measurements on dark side we increased the voltage applied to a PMT in order to increase the lidar sensitivity.[4] Some measurement sessions have been carried out at the station orientation that differed from the ICS2 by the direction of the station axis $+O_bX_b$ which, in these cases, was not in the orbit plane making an angle of up to several degrees with it. This orientation mode is periodically used to provide uniform heating of the station elements with the Sun thus improving the heat regime inside the station. Such an orientation is very unfavorable for lidar operation, because even in the middle of illuminated portion of the orbit (see Fig. 2*a*) when the slant range is minimum the lidar optical axis makes an angle of 5 to 10 degrees with the nadir direction. All this makes the distance to the objects sounded longer and return signals weaker. In the last measurement session the laser didn't reach its standard operation mode and, as a result, the recorder has recorded only noise (presumably the background noise).

TABLE II. Information on the experiments (1996).

No.	Date	Time (DMT) start / end	Number of cycles	Rel. meas. / false resp. (returns from clouds)	Orientation mode	Coordinates			Elevation angle, degs.		Remarks
						B_s, degs.	L_s, degs.	Cloudiness	Sun	Moon / phase	
1	13.02.96	13:26:00 / 13:27:45	20	??	ICSa	−41.51 / −38.25	45.58 / 51.01	moderate	< −15,0	–	No telemetric information
2	14.02.96	17:12:00 / 17:13:45	20	14/2 (0)	»	−34.36 / −29.80	353.81 / 359.14	»	60÷58	–	–
3	15.02.96	10:09:30 / 10:10:49	20	8/3 (2)	»	−31.77 / −26.97	98.69 / 103.81	dense	61÷60	–	–
4	16.02.96	12:07:59 / 12:09:44	20	2/6 (1)	»	−51.74 / −50.88	5.50 / 15.83	»	38÷44	–	EME in telemetric channel
5	17.02.96	18:58:00 / 18:59:44	20	0/8 (0)	»	−50.34 / −48.25	269.80 / 279.17	»	42÷48	–	–
6	18.02.96	10:23:26 / 10:25:10	20	??	ICS	−48.83 / −46.35	42.09 / 50.72	»	45÷51	–	No telemetric information
7	19.02.96	11:02:01 / 11:03:46	20	1/10 (0)	»	−48.39 / −45.55	28.06 / 36.66	»	43÷49	–	–
8	20.02.96	10:09:01 / 10:10:46	20	0/0 (1)	»	−46.62 / −43.34	41.54 / 49.51	»	44÷51	–	Failure in the range finder channel
9	26.02.96	18:08:03 / 18:13:29	60	6/0 (1)	OCSc	−4.56 / 39.00	123.79 / 136.27	»	< −70	12÷−6 / 0.50	–
10	01.03.96	09:54:56 / 10:00:21	60	60/0 (19)	»	−7.18 / −23.36	227.22 / 240.01	moderate	< −55	66÷42 / 0.86	Enhanced voltage at PMT
11	02.03.96	10:35:04 / 10:40:30	60	54/0 (6)	»	−13.17 / −28.96	215.94 / 229.77	»	< −50	63÷44 / 0.91	»
12	05.03.96	15:42:02 / 15:47:28	60	54/1 (2)	»	−35.29 / −46.92	143.17 / 165.24	»	< −37	43÷40 / 1.00	»
13	18.03.96	10:25:00 / 10:30:26	60	57/0 (24)	»	−44.09 / −28.44	242.54 / 265.34	»	< −43	−42 / 0.0	»
14	30.03.96	14:57:58 / 15:03:24	60	53/0 (11)	»	−38.79 / −24.41	111.37 / 128.30	thin	< −17	37÷54 / 0.80	»
15	31.03.96	14:03:56 / 14:09:22	60	58/0 (12)	»	−38.10 / −23.57	120.25 / 136.88	moderate	< −15	34÷54 / 0.87	»
16	01.04.96	14:44:14 / 14:49:40	60	45/2 (13)	»	−32.39 / −16.96	112.16 / 126.83	thin	< −17	34÷55 / 0.93	»
17	02.04.96	13:50:59 / 13:56:26	60	56/1 (11)	»	−29.44 / −13.64	123.27 / 137.24	»	< −16	28÷46 / 0.97	»

In February 1996 we started a new series of spaceborne lidar experiments. Table II gives brief information about the measurements sessions carried out. The majority of reliable measurements have been carried out on the dark side of the Earth in the OCSc orientation mode and with the enhanced voltage applied to the PMT. Unfortunately no telemetric information was available on some measurement sessions because of organizational faults at the SFC.

It should be noted that false responses took place sometimes in the range finder channel from the background noise when the Moon was full or its phase exceeded 0.9. Soundings of the Earth made in the orientation mode ICS2 on the high-latitude portions of the orbit (above 45°) under conditions of high cloud fraction and high Sun gave only few representative results in the range finder channel of the lidar.

6. SOME PRELIMINARY RESULTS OF THE EXPERIMENTS

Some results of range finding of the ocean surface are shown in Fig. 6, where they are divided into two groups. The left-hand portion of the figure presents data obtained along the direction close to nadir, while the right-hand side presents similar data obtained when approaching nadir. In order to provide a comparison between different experiments time of measurements is shown along X axis with its origin being at the moment of the first shot in a cycle the 20th being at 105 s. Solid lines in this figure show the calculated $D_c(t)$ values and bars show the measurement results D_m. The latter results involve the one-second time uncertainty because of nonintegral period between the shots. Detailed analysis of the dependence $D_c(t)$ reveals two main

factors. First of all the ellipticity of the station orbit contributes about 10 m/s change in $H_c(t)$ and second in the orientation mode ICS2 the lidar optical axis undergoes continuous variation of its position (the angle γ between it and the nadir direction) as one can see from Figs. 2*a* and 3. Joint effect of these two factors results in the situation when the minimum in calculated slant range $D_c(t)$ is reached not for minimum γ. The sign of the derivative dH_c/dt is different in different portions of the orbit, so the extremum in $D_c(t)$ may occur at 5 to 10 seconds before or after the extremum in $\gamma(t)$.

The systematic error is first of all caused by the fact that the value D_m is measured from the surface of the first lens of the lidar optical transmitter while the value D_c is measured from the station center of mass that makes an error of 12 m. Then the uncertainty ($\Delta\alpha \approx 0.3°$) in the direction of the lidar optical axis with respect to the station axes also contributes into the systematic error. And finally, there is an uncertainty in the calculated value D_c that can reach 150 m according to data of the radar control and should be added to the above two errors. The points where the trend in D_m intersects the curve $D_c(t)$ in two sessions of the spaceborne lidar experiment (curves *2* and *5*) are indicative of the fact that at these moments in time the actual and calculated positions of the lidar optical axis are on the opposite sides of the orbit plane at equal, in absolute value, angles.

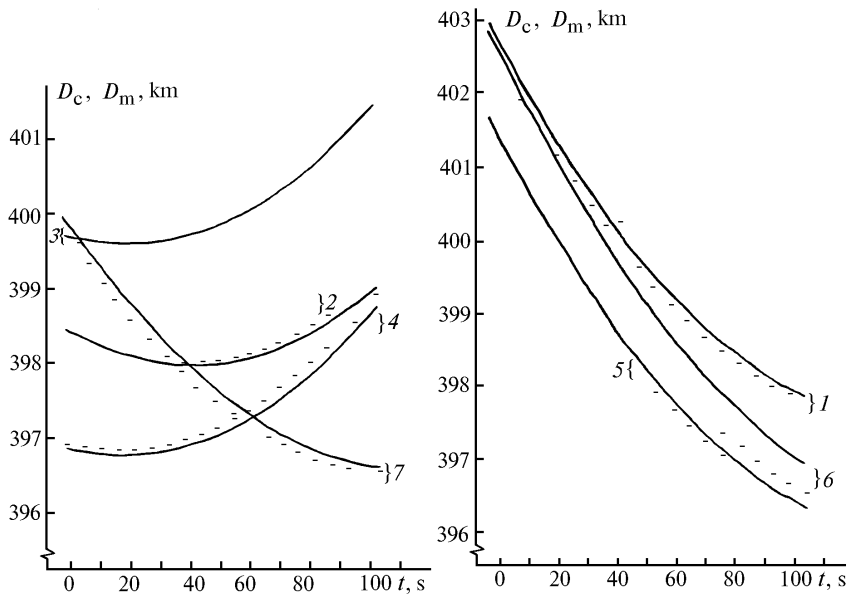

FIG. 6. Variations of the sounding range in the experiments conducted in the ICS2 orientation mode: 1 — 08.09.95; 2 — 09.09.95; 3 — 12.09.95; 4 — 15.09.95; 5 — 18.09.95; 6 — 21.09.95; 7 — 24.09.95.

Typical profiles of the height of the upper cloud boundary and of the range to the underlying surface obtained from observations over southern part of the Pacific ocean are shown in Figs. 7*a* and 7*b*. The *X* axis in these figures presents the number of measurements in a session and dots represent measurement data. In the former case (see Fig. 7*a*) one can see the fields of low level broken clouds while in the latter one the clouds of both low and upper level are seen. According to the meteorological bulletin, in the beginning of this path there were observed cumulus clouds (5–8 cloud fraction with the low boundary at 600 to 1000 m height). In the middle portion of the path there was stratocumulus cloudiness (5–8 cloud fraction with the low boundary at 600 to 1000 m height) and in the end of the path there was observed the stratocumulus cloudiness (3–6 cloud fraction with the low boundary at 1000 to 1500 m height). The clouds of both the low and upper level were observed with the lidar on March 18, 1996 (Fig. 7*b*) with only high clouds near the middle of the path. In that case, according to the meteorological bulletin, in the beginning of the path there were observed stratocumulus clouds (6–9 cloud fraction with the low boundary at 300 to 600 m height). In the middle portion of the path there were cumulus clouds (3–6 cloud fraction with the low boundary at 600 to 1000 m height) and in the end of the path there were observed isolated cumulus clouds (0–3 cloud fraction with the low boundary at 1000 to 1500 m height). Taking into account the global nature of meteorological data and the fact that lidar estimates the height of the upper boundary while in meteorological information we have data on the low boundary of the clouds the agreement between the data may be considered as satisfactory. In some measurement cycles the amplitude of lidar returns was below the first amplitude threshold and thus it was not recorded. Such events are marked on the figure by the word "NO". This is characteristic of the cloudiness with high upper boundary.

Figure 7*c* presents lidar data obtained over Australia and partially over the see surface (see Fig. 5 and Table II). At that time there were observed high clouds (at about 10 km height) over the central and

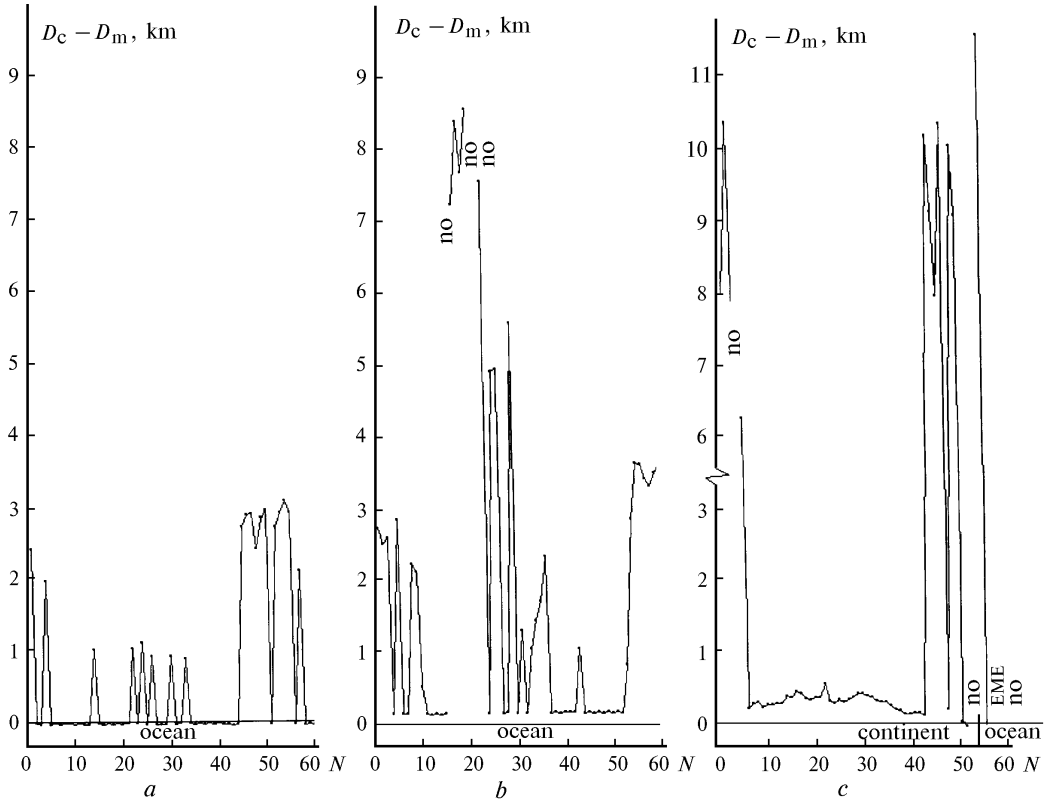

FIG. 7. The profiles of the upper boundary height of clouds and of the distance to the underlying surface measured in the orientation mode OCSc at the dark side of the Earth: a) 01.03.96*; b)* 18.03.96*; c)* 02.04.96.

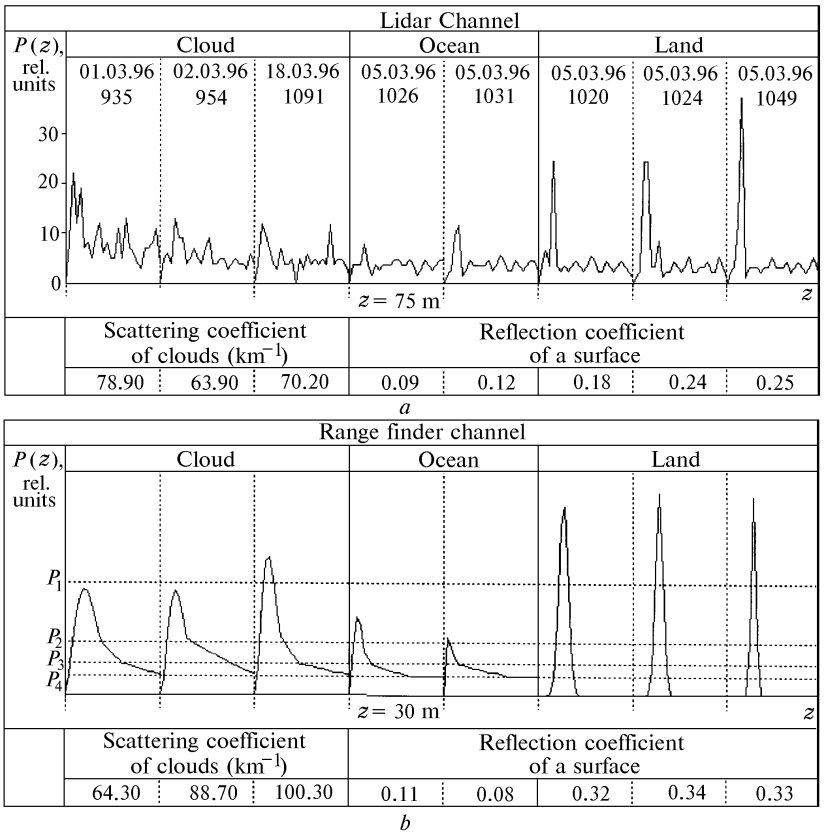

FIG. 8. The profiles of lidar returns from different scattering objects as reconstructed from the data of the lidar (a) and range finder (b) channels.

northern part of this continent. There was one false record detected at high and nearly full Moon from the background noise. According to the meteorological bulletin, in the beginning of this path there were observed cirrus clouds (0–3 cloud fraction with the low boundary at a height above 2.5 km). In the middle portion of the path there was stratocumulus cloudiness (1–4 cloud fraction with the low boundary at 1000 to 1500 m height) and in the end of the path there was observed the cumulostratus cloudiness (3–6 cloud fraction with the low boundary at 600 to 1000 m height). In this lidar experiment the discrepancies observed between the lidar and meteorological data were too large. One interesting fact should be mentioned here. During four days since March 30 and until April 2, 1996 we have observed with the lidar a stationary cloud field over the Australian desert at a height of 7 to 12 km.

The systematic measurement error (the difference between D_c and D_m at the ocean level) varied from session to session both in sign and magnitude because of the above discussed reasons. Moreover, as the detailed analysis has shown, there may occur shot to shot variations of this error. On the whole, the agreement between the lidar and meteorological data in other sessions were similar to the above mentioned. It should be noted that false records were detected in the range finder channel when working on the dark side of the orbit over the shore regions of the ocean.

Figure 8 presents examples of return signals from cloud formations, water surface, and land. Figure 8*a* shows return signals recorded with the lidar channel and Fig. 8*b* the signals recorded with the range finder channel. Horizontal axis in these figures presents the range scale. Power of return signals is shown along the vertical axis in relative units. In the case of the range finder channel the return intensity is presented by the power thresholds of the recorder. As is seen from Fig. 8 return signals from clouds and land are the strongest. The return signals from ocean surface are between the second and third threshold. The majority of lidar returns from the atmosphere are from sufficiently dense cloud formations what is well illustrated by the values of the scattering coefficient also presented in the figure. This results in a small number of amplitude readouts in a return signal what requires some special data processing algorithms to be used in this case.

7. CONCLUSION

The above discussed cycles of experiments conducted with the spaceborne lidar "Balkan" have clearly demonstrated its functional ability and good agreement between its actual and calculated specifications. The vertical spatial resolution of 3 m is a record value for the spaceborne sounders. Use of a range finder channel (it measurement error is ±1.5 m) enables one to improve by an order of magnitude the accuracy of the orbit height measurements as compared to the radar measurements currently in use.

The methodology of planning the spaceborne lidar experiments and organizing their ground support measurements from the SFC have been developed. The experience of these experiments, together with the possibilities of replacing some lidar blocks for updated ones in future missions, allow us to be optimistic about the possibility of improving the quality of lidar data to be obtained. Finally we'd like to mention that the experience of work with the lidar "Balkan" appeared to be very valuable for the development of future generation "Balkan" lidars.

ACKNOWLEDGMENTS

The authors would like to acknowledge the astronauts from the missions EO-19, EO-20, and EO-21 for their excellent and highly professional work with the lidar during the lidar experiments onboard the orbiting station "Mir". We are also thankful to our colleagues from the group of mathematical modeling at the SFC for the software they provided, as well as for the ballistic calculations they made for this experiment.

It is our pleasure to thank Dr. A.I. Mangel and many other employers from the SFC who contributed to arrangement and performance of the first Russian spaceborne lidar experiment.

REFERENCES

1. M.P. McCormick, D.M. Winker, E.V. Browell et al., Bull. Meteorol. Society **74**, No. 2, 205–214. (1993).
2. Yu.S. Balin, V.V. Burkov, I.V. Znamenskii, et al., Abstracts of the 15th Intern. Laser Radar Conf. (Tomsk, 1990), Vol. 1, pp. 12–14.
3. Yu.S. Balin, V.E. Mel'nikov, A.A. Tikhomirov, et al. Proc. SPIE **2310**, *Lidar Tecniques for Remote Sensing,* 144–151 (1994).
4. Yu.S. Balin, I.V. Znamenskii, V.E. Zuev, et al., Atmos. Oceanic Opt. **8**. No. 9, 711–717, 1995.
5. The Technique P24586-117. Part 1. Book 1. S&PA "Energiya", 1986, 48 pp.
6. A.I. Abramochkin, I.E. Penner, V.S. Shamanaev Atm. Opt. **4**, No. 3, 264–265 (1991).
7. V.M. Zakharov ed., *Laser Sensing of the Atmosphere from Space* (Gidrometeoizdat, Leningrad, 1988), 215 pp.
8. J.L. Bufton Proceedings of the IEEE **77**, No. 3, 463–477 (1989).
9. V.E. Zuev, Yu.S. Balin, V.V. Zuev, et al., Atmos. Oceanic Opt. **8**, No. 12, 949–954 (1995).